

**AFRL-PR-WP-TR-2006-2079**

**HIGH GRAVITY (g) COMBUSTION**

**Dr. Joseph Zelina**

**Combustion Branch (AFRL/PRTC)**

**Turbine Engine Division**

**Propulsion Directorate**

**Air Force Materiel Command, Air Force Research Laboratory**

**Wright-Patterson Air Force Base, OH 45433-7251**



**FEBRUARY 2006**

**Final Report for 10 February 1999 – 28 February 2006**

**Approved for public release; distribution is unlimited.**

**STINFO FINAL REPORT**

**PROPULSION DIRECTORATE**

**AIR FORCE MATERIEL COMMAND**

**AIR FORCE RESEARCH LABORATORY**

**WRIGHT-PATTERSON AIR FORCE BASE, OH 45433-7251**

# NOTICE

Using Government drawings, specifications, or other data included in this document for any purpose other than Government procurement does not in any way obligate the U.S. Government. The fact that the Government formulated or supplied the drawings, specifications, or other data does not license the holder or any other person or corporation; or convey any rights or permission to manufacture, use, or sell any patented invention that may relate to them.

This report was cleared for public release by the Air Force Research Laboratory Wright Site (AFRL/WS) Public Affairs Office (PAO) and is releasable to the National Technical Information Service (NTIS). It will be available to the general public, including foreign nationals.

PAO case number: AFRL/WS 04-0258

Date cleared: 02 Jul 2004

THIS TECHNICAL REPORT IS APPROVED FOR PUBLICATION.

//S//

---

JOSEPH ZELINA, Ph.D.  
Project Monitor  
Combustion Branch

//S//

---

ROBERT D. HANCOCK, Ph.D.  
Chief  
Combustion Branch

//S//

---

JEFFREY M. STRICKER  
Chief Engineer  
Turbine Engine Division  
Propulsion Directorate

This report is published in the interest of scientific and technical information exchange and its publication does not constitute the Government's approval or disapproval of its ideas or findings.

# REPORT DOCUMENTATION PAGE

*Form Approved*  
OMB No. 0704-0188

The public reporting burden for this collection of information is estimated to average 1 hour per response, including the time for reviewing instructions, searching existing data sources, gathering and maintaining the data needed, and completing and reviewing the collection of information. Send comments regarding this burden estimate or any other aspect of this collection of information, including suggestions for reducing this burden, to Department of Defense, Washington Headquarters Services, Directorate for Information Operations and Reports (0704-0188), 1215 Jefferson Davis Highway, Suite 1204, Arlington, VA 22202-4302. Respondents should be aware that notwithstanding any other provision of law, no person shall be subject to any penalty for failing to comply with a collection of information if it does not display a currently valid OMB control number. **PLEASE DO NOT RETURN YOUR FORM TO THE ABOVE ADDRESS.**

<b>1. REPORT DATE (DD-MM-YY)</b> February 2006		<b>2. REPORT TYPE</b> Final		<b>3. DATES COVERED (From - To)</b> 02/10/1999 – 02/28/2006	
<b>4. TITLE AND SUBTITLE</b> HIGH GRAVITY (g) COMBUSTION				<b>5a. CONTRACT NUMBER</b> In-house	
				<b>5b. GRANT NUMBER</b>	
				<b>5c. PROGRAM ELEMENT NUMBER</b> 61102F	
<b>6. AUTHOR(S)</b> Dr. Joseph Zelina				<b>5d. PROJECT NUMBER</b> 2308	
				<b>5e. TASK NUMBER</b> S7	
				<b>5f. WORK UNIT NUMBER</b> XY	
<b>7. PERFORMING ORGANIZATION NAME(S) AND ADDRESS(ES)</b>  Combustion Branch (AFRL/PRTC) Turbine Engine Division Propulsion Directorate Air Force Materiel Command, Air Force Research Laboratory Wright-Patterson Air Force Base, OH 45433-7251				<b>8. PERFORMING ORGANIZATION REPORT NUMBER</b>  AFRL-PR-WP-TR-2006-2079	
<b>9. SPONSORING/MONITORING AGENCY NAME(S) AND ADDRESS(ES)</b>  Propulsion Directorate Air Force Research Laboratory Air Force Materiel Command Wright-Patterson AFB, OH 45433-7251				<b>10. SPONSORING/MONITORING AGENCY ACRONYM(S)</b> AFRL-PR-WP	
				<b>11. SPONSORING/MONITORING AGENCY REPORT NUMBER(S)</b> AFRL-PR-WP-TR-2006-2079	
<b>12. DISTRIBUTION/AVAILABILITY STATEMENT</b> Approved for public release; distribution is unlimited.					
<b>13. SUPPLEMENTARY NOTES</b> Report contains color.					
<b>14. ABSTRACT</b>  Ultra-short combustors to minimize residence time, with special flame-holding mechanisms to cope with increased through-velocities are likely in the future. The Ultra-Compact Combustor (UCC), a novel design based on trapped-vortex combustor (TVC) work that uses high swirl in a circumferential cavity to enhance reaction rates via high cavity g-loading on the order of 3000 g's. Increase in reaction rates translates to a reduced combustor volume. Three combustor geometric features were varied during experiments (1) high-g cavity flame-holding method, (2) high-g cavity to main airflow transport method, and (3) fuel injection method. Results have shown promise for advanced engine applications. Lean blowout fuel-air ratio limits at 25-50% the value of current systems were demonstrated. Combustion efficiency was measured over a wide range of UCC operating conditions. This data begins to build the design space required for future engine designs that may use these novel, compact, high-g combustion systems.					
<b>15. SUBJECT TERMS</b> combustion, compact combustion, trapped vortex combustion, high gravity combustion					
<b>16. SECURITY CLASSIFICATION OF:</b>			<b>17. LIMITATION OF ABSTRACT:</b> SAR	<b>18. NUMBER OF PAGES</b> 30	<b>19a. NAME OF RESPONSIBLE PERSON (Monitor)</b> Dr. Joseph Zelina <b>19b. TELEPHONE NUMBER (Include Area Code)</b> (937) 255-7487
<b>a. REPORT</b> Unclassified	<b>b. ABSTRACT</b> Unclassified	<b>c. THIS PAGE</b> Unclassified			

## **ABSTRACT**

Future gas turbine engines are required to be more capable than their predecessors. This often implies severe demands on the engine that translate into increasing compressor and combustor exit temperatures, higher combustion pressures and higher fuel/air ratio combustors with greater turn-down ratios (wider operating limits between idle and maximum power conditions). Major advances in combustor technology are required to meet the conflicting challenges of improving performance, increasing durability and maintaining cost. Unconventional combustor configurations are one promising approach to address these challenges. Ultra-short combustors to minimize residence time, with special flame-holding mechanisms to cope with increased through-velocities are likely in the future. This paper focuses on vortex-stabilized combustor technologies that can enable the design of compact, high-performance combustion systems. Compact combustors weigh less and take up less volume in space-limited turbine engine for aero applications.

This paper presents a parametric design study of the Ultra-Compact Combustor (UCC), a novel design based on trapped-vortex combustor (TVC) work that uses high swirl in a circumferential cavity to enhance reaction rates via high cavity g-loading on the order of 3000 g's. Increase in reaction rates translates to a reduced combustor volume. Three combustor geometric features were varied during experiments which included (1) high-g cavity flame-holding method, (2) high-g cavity to main airflow transport method, and (3) fuel injection method. Experimental results are presented for these combustor configurations and results have shown promise for advanced engine applications. Lean blowout fuel-air ratio limits at 25-50% the value of current systems were demonstrated. Combustion efficiency was measured over a wide range of UCC operating conditions. This data begins to build the design space required for future engine designs that may use these novel, compact, high-g combustion systems.

## **ACKNOWLEDGMENTS**

The authors are grateful to Mr. Glen Boggs, Mr. Ron Britton and Mr. Stephen Britton for their assistance in fabrication, assembly and test of the combustion rigs, and to Mr. Jeffrey S. Stutrud for assistance with the data acquisition system. This work is supported in part by Air Force Office of Scientific Research (AFOSR) with Dr. Julian Tishkoff serving as Program Manager.

## INTRODUCTION

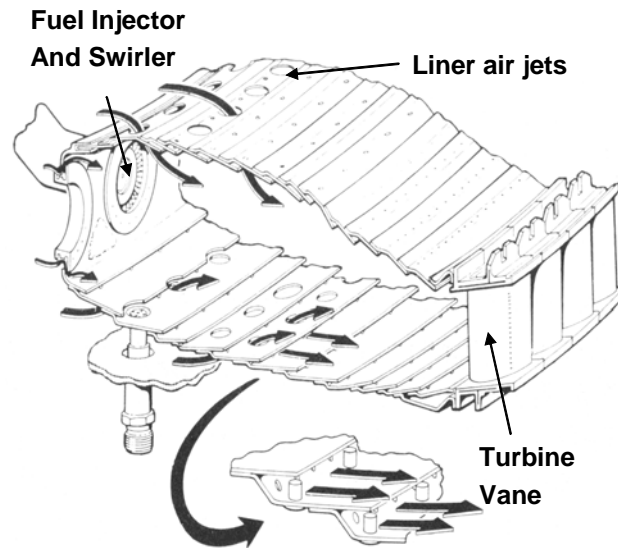
To meet the conflicting requirements of higher compression ratio, high peak temperatures, reduced weight and low emissions, with improved engine durability requires revolutionary combustion systems. For example, advanced combustors are becoming shorter and utilize non-metallic materials to meet the required thrust-to-weight ratio goals. Shorter residence times in the combustion chamber may reduce the NO<sub>x</sub> emissions, but the CO and UHC emissions then increase due to inadequate reaction time. Also, the partially-reacted fuel could escape the combustion chamber and continue to burn in the turbine machinery, which could pose a series of rotating component challenges such as vane and blade durability, and pressure loss increases.

To meet these challenges, novel approaches to combustion system design have been underway at the Air Force Research Laboratory (AFRL) to investigate compact combustion systems. These systems employ improved mixing devices, geometric features to expand combustor operability<sup>1,2,3</sup>, and dramatic changes to combustor flowfields to reduce combustor size and pollutant emissions<sup>4-8</sup>. This paper focuses on vortex-stabilized combustor technologies that can enable the design of compact, high-performance combustion systems. Work in this area by the Air Force began around 1993 with vortex-stabilized flames held in mechanical cavities. Much of this work has fallen under the broad title of Trapped Vortex Combustor (TVC) technology.

Experiments have begun on a possible ultra-compact combustor (UCC) concept which will combine the combustor with the compressor exit guide vanes and the turbine inlet guide vanes. To illustrate the uniqueness of this concept, a segment of a conventional annular combustor is shown in Fig. 1. Air enters the combustion chamber through dome swirlers and liner holes that provide mixing air and cooling air to the system. In conventional design, the residence time in the combustor is a function of axial length of the system; therefore, engine length is needed to complete the combustion process. The mixture is burned, and then exits the combustor through turbine inlet guide vanes, which direct the flow at the correct angle at the high pressure turbine rotor. In a typical system, the air exiting the compressor is de-swirled and decelerated before entering the combustion system plenum. The air is then locally re-swirled in the combustion chamber to promote mixing and flame stabilization, and then the flow is turned once again and accelerated before entering the turbine, with each of these processes taking place in the engine axial direction.

In the UCC concept, a cavity runs around the outer circumference of the extended turbine inlet guide vanes, as seen in the segment of Fig. 2. All of the fuel is introduced into this cavity. Aligned with this cavity, on each vane, will be a radial cavity that extends to the inner platform. The idea is to burn rich in the circumferential cavity, allowing much of the required combustion residence time to take place in the circumferential direction of the engine, rather than the axial as is done conventionally. The flow within this cavity will be swirled to generate high “g” loading and improve fuel-air mixing<sup>4,8</sup>. Flame stabilization occurs as combustion products are recirculated in the cavity. The intermediate products of combustion are transported by lower wake pressures into the radial cavities in the vane surfaces where combustion continues at a reduced equivalence ratio as the mainstream air is entrained into the wakes. Finally, across the leading edge of the vanes, again in a circumferential

orientation, there may be a minimum blockage flame-holder (if necessary) where products will be entrained and distributed into the main flow.



(Schematic from “*The Aircraft Gas Turbine and its Operation,*” P&W Oper. Instr.200, Pratt & Whitney, United Technologies.)

**Figure 1: Conventional Gas Turbine Combustor.**

Functionally, the circumferential cavity may be regarded as a primary zone, the radial cavities as constituting an intermediate zone, and the circumferential strut flame-holder as the dilution zone. All combustion is intended to be completed prior to any flow turning and acceleration caused by the turbine inlet guide vanes. Swirl from either the compressor (if used as a main combustor) or the turbine stage ahead of the ITB may be used to drive the swirl in the circumferential cavity. Using the compressor swirl will negate the need for a stator ahead of the combustor, further shortening overall system length.

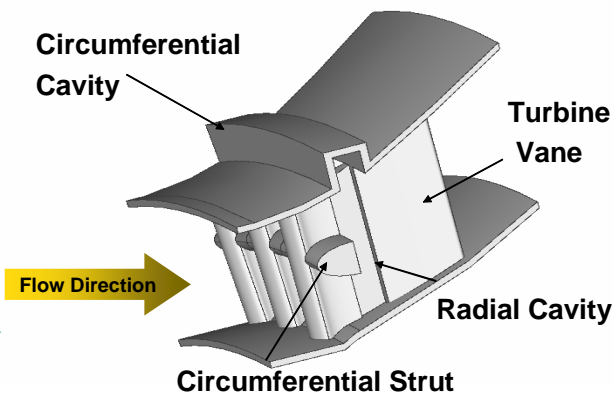


**Figure 2: Ultra-Compact Combustor Concept Showing Integral Circumferential Cavity and Turbine Vanes.**

The cavities are a folded combustion system so that the rich-burn, quick-quench, lean-burn (RQL) process starts at the inlet of the combustor with the rich burn process taking place in

parallel with the lean burn, and is accomplished without extending the length of the combustion system. It has been estimated that such an ultra-compact combustor would be at least 50% shorter than a conventional combustion system when defined as the diffuser, combustor, and the turbine inlet guide vanes. Note that the former vane leading-edge showerhead, traditionally a durability item, in the UCC form serves as an air-intake to provide cooling air for the vane radial cavities. To keep the weight of the extended chord vane pack reasonable, use of high temperature composites are considered for construction. The overall pressure drop of the system will be determined by the cooling needs of the rear portions of the vanes, and of the circumferential main cavity.

## BACKGROUND

The design of UCC using high g-loading came about by realization of earlier experiments on combustion and high g loading by Lewis<sup>9</sup>. In an attempt to increase the flame speed to a value beyond that of a turbulent flame, Lewis<sup>9</sup> has investigated the role of centrifugal forces on flame spreading. Using a combustion-centrifuge device, shown in Fig. 3, he established centrifugal forces up to  $10^4 g_0$  and observed flame speeds increasing nearly 4 times that of a conventional turbulent flame. Based on these results he argued that flames propagate in combustible mixtures in three modes; 1) laminar burning in which flame speed depends on the heat conduction and radical diffusion into fresh mixture, 2) turbulent burning in which turbulent transport of small elements of flame into the unburned mixture act as new ignition sources, and 3) bubble burning in which small packets of burnt gases raise through fresh mixture due to buoyancy and spread the flames surrounding them. The four-fold increase in flame speeds from conventional turbulent values without having to increase the inlet velocities is quite lucrative and one should explore such techniques in ITB where rapid combustion in the cavities is required.

Lewis<sup>9</sup> experimental results are shown in Fig. 5. He found that for propane-air mixtures, the flame propagation rate remained nearly constant at 18 ft/sec (~5 m/sec) up to about 200 g's. For values of 500-3500g's, the flame speed increases as the square root of the g-loading up to nearly 60 ft/sec (18 m/sec). What is very interesting in the data shown in Fig. 4 is that the observed flame speed is much higher than documented turbulent flame speeds. For example, maximum laminar flame speed for propane-air mixtures is  $S_L \sim 0.43$  m/sec with corresponding maximum turbulent flame speed around 2 m/sec. Therefore, based on the Lewis<sup>9</sup> data at high g-loads, the flame speed is as much as 3-4 times the turbulent flame speed of the mixture. Lewis<sup>9</sup> attributed the increased flame speed to the turbulent enhancement due to "bubbles" or eddies that move ahead of the flame front due to the centripetal acceleration. Lewis<sup>9</sup> describes this process in Fig. 5. In the picture on the left, the bubble or eddy velocity exceeds the turbulent flame speed and the flame propagates at the eddy velocity. On the right is a visualization of the case where the eddy velocity is lower than the turbulent flame speed and the mixture propagates at the turbulent flame speed.



gravitational force is imposed along the length. Flame is initiated at the bottom of the tube by providing three ignition sources. Calculations are repeated by changing the applied gravitational force between  $0g_0$  and  $500g_0$ .

Results obtained for  $10g_0$  and  $500g_0$  cases are shown in Figs. 6a and 6b, respectively. For each case two-dimensional flame structures in the tube at three instants are shown. When the applied gravitational force is small (less than  $\sim 10g_0$ ) the individual flamelets initiated from the three ignition sources merged quickly and resulted in a uniform flat flame across the tube. The propagation velocity of this flat flame is  $\sim 1.86$  m/s, which is close to the laminar burning velocity in the 0.8-equivalence-ratio  $H_2$ /air mixture. Even though, the propagation velocity of the individual flamelet is increasing with the gravitational force the velocity of the flat flame (formed after mixing of flamelets) is independent of the applied gravitational force. When gravitational force is increased to  $500g_0$ , as seen in Fig. 6b, a mushroom vortex is formed due to small differences in the initial flamelets. The buoyancy acting on the light combustion products contained in the vortex propelled the vortex and the flame around it at a significantly higher speed. The propagation velocity of the flame in this case reached 9.2 m/s, that is  $\sim 5$  times that of the laminar burning velocity. The simulation in Fig. 6b confirms the bubble-transport hypothesis proposed by Lewis<sup>9</sup>, however, in a laminar flow situation. It may be argued that turbulence is a small-scale phenomenon and modifies (increases) the local burning velocity along the flame front. Consequently, in a turbulent-flow environment the flat flame in Fig. 6a propagates at the turbulent flame speed and the flame around the vortex in Fig. 6b propagates at turbulent burning velocity plus the bubble velocity.

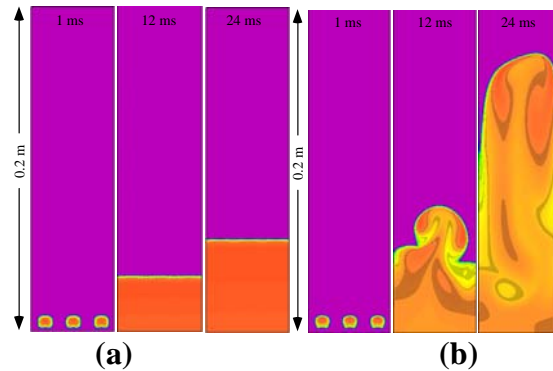


**Figure 6: Spreading of Flame Under a Gravitational Force of (a)  $10g$  and (b)  $500 g$ 's.**

The propagation velocity obtained at different gravitational forces are shown in Fig. 7. The initial plateau region corresponds to the flamelet-merging phenomenon and the latter steep-rise region corresponds to the bubble-transport phenomenon. Lewis<sup>9</sup> in his centrifuge experiment noted flame velocities that are greater than the values expected from “bubble-transport” hypotheses and he attributed this overshoot in velocity to the thermal expansion of the hot gases. If that is true, then such phenomenon can occur only in enclosed tubes such as the ones used by Lewis<sup>9</sup> and in the numerical experiment described here. However, such an enclosed environment may not arise in the cavities of the ITB due to the large width-to-length ratio. Experiments have shown that the ITB can operate with very high efficiencies and extremely short flame lengths (see Fig. 11b). Therefore, in order to make use of the benefits

of the centrifugal-force effects on combustion, we must perform fundamental studies that are appropriate for the diffusion flame swirling flows in cavities with large width-to-length ratios.

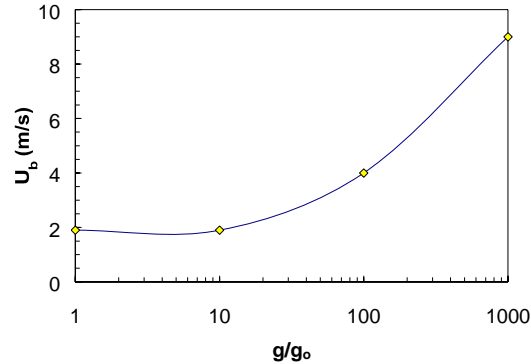


**Figure 7: Flame Speed Determined at a Height of 0.18 mm for Different Gravitational Forces.**

## **SETUP**

### **The Test Facility**

The Air Force Research Laboratory (AFRL) Atmospheric Pressure Combustor Research Complex (APCRC) can supply a total of up to 0.75 lbm/sec of heated air at atmospheric pressure, with three independently controllable air systems available to allow for different air splits to be separately supplied to the combustor. The air can be electrically heated to temperatures ranging from room temperature to 600 °F. Two independently controlled fuel systems are available, each supplying flow at up to 400 psia and 5 lbm/min flow rate. The facility is fully instrumented for pressure, temperature and flow rates. Emissions analyzing equipment is available to detect CO, CO<sub>2</sub>, NO<sub>x</sub>, O<sub>2</sub>, and total unburned hydrocarbons (UHC) at the combustor exit plane. Emissions were collected with a 5-element oil-cooled probe located at the exit of the rig.

### **Combustor Rig Design**

The UCC rig has simulated turbine inlet guide vanes, and is shown in Fig. 8. Basic dimensions of the configuration tested are also shown in this figure. The circumferential cavity width is 1.5 inches. The rig uses a 1.95” diameter centerbody.. The fuel is introduced in the cavity at 6 discrete injection sites equally spaced around the circumference. The fuel is injected radially inward using standard pressure atomizing fuel injectors. Air is injected into the cavity at a 45 degree angle and at 24 locations to create the bulk circumferential swirl in the cavity. The jets are 0.213” diameter. Main air flows axially over the circumferential cavity (separate air circuit than the cavity airflow) where entrainment, which can be substantial, induces a spiral flow trajectory within the cavity.

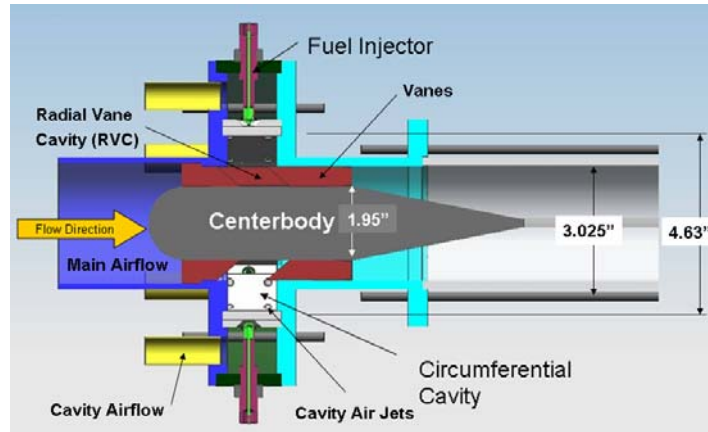


**Figure 8: Schematic of the UCC Rig Showing Complete Flowpath and Cavity/Vane Placement and Fuel /Air Injection Locations.**

The cavity mixture partially burns and is transported to the axial main air zone, where the mixture is diluted and reactions continue to completion. In the rig, transport out of the circumferential cavity takes place along the vanes and inside the radial vane cavity (RVC) located on the vanes. A photograph of the assembled combustor rig, including fuel and air feed manifolds, centerbody, vanes, and inlet plenum is shown in Fig. 9. Notice that a quartz extension plenum is added to the combustor exhaust portion to allow for optical access into the combustor cavity and vane location.

### **Test Conditions**

The three different test configurations are described in Table 1. In all cases, the same pressure-atomizing fuel injectors were used for all configurations. Airflow around the fuel injector was varied by moving the tapered fuel injector away from the circumferential cavity wall. This can be seen in Fig. 10a, where a large gap is seen between the pressure-atomizing fuel injector and the opening to the circumferential cavity. In Fig. 10b, this gap is minimized to reduce the airflow. The other parameter that was changed was the shape of the RVC. The vane designs, along with the two RVC features are shown in Fig. 11. Figure 11a shows the angled RVC design, and Fig. 11b shows the contoured design. The modification, shown in Fig. 11b, was done in an attempt to prevent acoustics and to reduce pressure loss along the main airflow stream. The data will show, however, that the radial transport was negatively impacted using this design compared to the original angled RVC. The radial vane cavity was located on the side of the vane downstream of the circumferential flow.

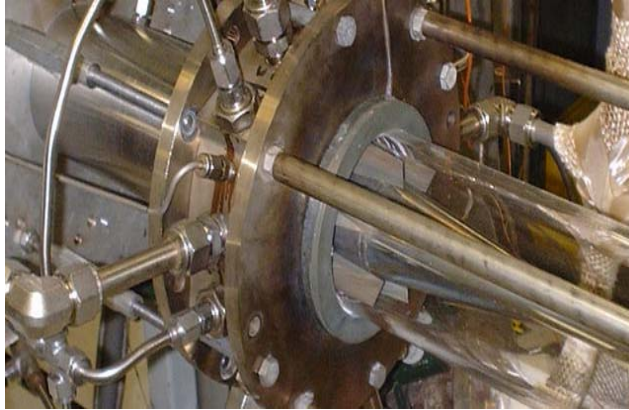


**Figure 9: Photograph of the assembled Ultra-Compact Combustor (UCC) rig.**

**Table 1: Combustor Design Configurations.**

Configuration	Injector Air (% total)	RVC Design
1	1.5	Contoured
2	1.5	Angled
3	0.3	Angled



**(a)**



**(b)**

**Figure 10: Fuel Injector airflow with (a) high air around fuel injector and (b) low air around fuel injector.**

The tests were run at combustor pressure drops in the range from  $1\% < dP/P < 4\%$ , and overall fuel/air ratios (OFAR) in the range  $0.0075 < \text{OFAR} < 0.02$ , (equivalent to  $0.6 < \phi_{\text{cav}} < 2.1$ ), with a fixed inlet temperature  $T_3$  of 500 °F. Liquid JP-8 + 100 fuel was used. Cavity airflow remained nearly constant, at 18% of the total airflow to the system. The variation was due largely to the different effective areas of the individual fuel injectors when immersed into the combustor at different depths. The airflow around the fuel injector is estimated to be 0.3-1.5% depending on the immersion depth. The cavity airflow includes air entering around the fuel injector as well as the cavity air jets. Typical flow ranges are shown in Table 2. Fuel injector Flow Number  $((\text{lb/hr})/(\text{psi})^{0.5})$  was 0.35 for each injector.

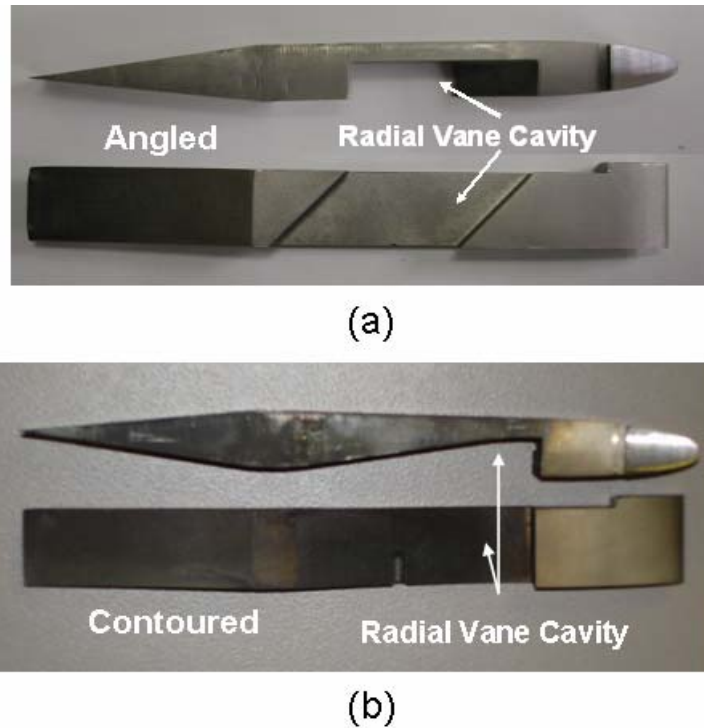


**Figure 11: Radial Vane Cavity (RVC) design showing (a) angled and (b) contoured geometry.**

**Table 2: Typical UCC Operating Conditions.**

	<b>Wa Main</b> lb/min	<b>Wa Cavity</b> lb/min	<b>Wfuel</b> lb/min	$\phi$
<b>LBO Points</b>	9-25	1.6-5.6	0.014- 0.14	0.008- 0.4
<b>Efficiency Points</b>	6.6-15	1.3-3.86	0.085- 0.34	0.6- 2.1

### **Error Analysis**

Experimental error results from the combination in flow measurement error, temperature errors and emissions measurement equipment error. Estimated combined error for the UCC rig is +/- 6 percent. The highest error results from the airflow measurement to the rig's two air circuits.

## **RESULTS AND DISCUSSION**

### **Atomization Effects**

Recent work<sup>6</sup> with the UCC/ITB suggests a dependent behavior on reaction temperature and/or liquid fuel atomization, in addition to g-loading effects. Yonezawa et al.<sup>11</sup> introduced the observations for flame propagation by Chomiak<sup>12</sup> for turbulence enhancement through the generation and movement of non-premixed buoyant “bubbles”, or eddies, of non-premixed and partially-premixed reactants, and burned reactants, such that the burning velocity ( $S_b$ ),

$$S_b = \frac{\rho_u}{\rho_b} \sqrt{Rg} \quad \text{Eq. 1}$$

where the density gradient is worked on by the centrifugal force generated through the swirl. So, at fixed radius (R) and operating pressure, and neglecting differences in gas constants,

$$S_b \propto \frac{T_b}{T_u} \sqrt{g} \quad \text{Eq. 2}$$

$T_u$  is taken as the air inlet temperature and  $T_b$  ideally should be a measured gas temperature at the cavity exit, but here is taken as the adiabatic flame temperature calculated for JP-8/air from an equilibrium chemistry code. When found in these ways the ratio  $T_b/T_u$  represents a maximum value. Therefore, if combustion efficiency is assumed to be proportional to  $S_b$ , and when data is plotted in terms of  $(T_b/T_u)(g)^{1/2}$  as the abscissa, the systematic variation in the conditions for the maximum combustion efficiency should be eliminated, and improved correlation of combustion efficiency data would be expected, for cavity-only burning and if there are no physical effects controlling the combustion process. Fig. 12 shows the data-correlation attempt for one cavity design<sup>6</sup>. It can be seen that improved data correlation does not happen, except for very high values of  $(T_b/T_u)(g)^{1/2}$ , greater than 230, and for  $\phi_{cav}$  less than 1.3.

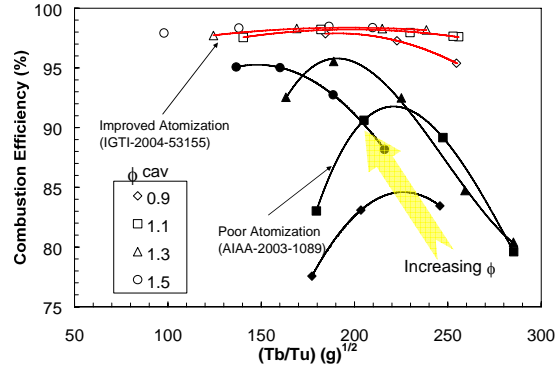


**Figure 12: Effects of Atomization Quality on the Correlation Parameter for High g Combustion.**

It is obvious from the nature of the correlation failure in Fig. 12 data (AIAA 2003-1089)<sup>6</sup> that at least one important process is unaccounted for in the simple theory. Characteristic time studies in the primary zones of conventional combustors at conditions similar to those of the present experiments<sup>13</sup>, always show that the times for liquid fuel evaporation and fuel vapor/air mixing are so much greater than any chemical reaction time, and therefore, control such measures of performance as combustion efficiency. Mixing in the cavity is enhanced by the g-forces, which leaves atomization as a possible cause. In the experiments, the g-loading was varied by changing the air pressure drop across the cavity such that higher g-loadings required higher air pressure drops. Similarly at given g-loading, increasing  $\phi_{cav}$  was done by increasing fuel mass flow rate. Based on spray data<sup>6</sup>, at low cavity equivalence ratios and low g-loading, the spray SMD is of the order of 55  $\mu\text{m}$  or greater for JP-8+100 physical properties, at low g-loadings but high  $\phi_{cav}$  the SMD is around 20  $\mu\text{m}$ , and for high g-loadings and all cavity equivalence ratios the SMD is less than 20  $\mu\text{m}$ . It is generally accepted that

sprays with SMD's around 15  $\mu\text{m}$  behave in combustion as though the fuel was introduced as a vapor. Evaporation rates are proportional to the square of SMD, and are also dependent on reaction temperature, reaching a maximum around peak temperatures. Therefore, the combustion efficiency is most likely influenced by liquid fuel spray atomization.

Additional tests were conducted<sup>7</sup> where the atomization level was increased by reducing the injector flow number and thereby increasing the fuel pressure drop across the fuel injector tip. Estimates of spray SMD were about 15-25  $\mu\text{m}$ . Plotting the data for these experiments in a similar fashion to Fig. 12, the curves tend to collapse, indicating that the atomization effects in the combustion device are a strong driver for system performance, and were the cause of the inability to correlate the combustion efficiency with Eq. 2. When atomization levels provide  $\sim 20 \mu\text{m}$  drops, the flame speed is dictated only by the cavity reaction temperature and the g loading. This data is shown in Fig. 12.

### Heat Release Rate

As mentioned previously, the UCC axial length is approximately 3 inches; significantly less length than conventional systems. In fact, the reduction in axial length is significant, since the reduced volume translates to increased heat release rates of the UCC compared to conventional combustion systems. Cavity space heating rate (HRR) was calculated for one experiment and plotted as a function of the cavity temperature rise and cavity pressure drop, as seen in Fig. 13. As expected, as the temperature rise increases in the cavity, the heat release rate increases. Interestingly, the HRR is also a strong function of the pressure drop. The data suggests that for a given HRR in the cavity, the cavity volume can be reduced while still maintaining a constant temperature rise if the pressure drop is increased. The HRR for the cavity is 20-40 MBtu/atm-ft<sup>3</sup>. Also plotted are data from two gas turbine engine manufacturers, estimating the primary zone space heating rate. Both combustion systems, from Company A and Company B, required a much higher primary zone temperature rise to reach the level of space heating rate of the UCC cavity. In general, the UCC operates at higher space heating rates compared to conventional gas turbine combustor primary zones.

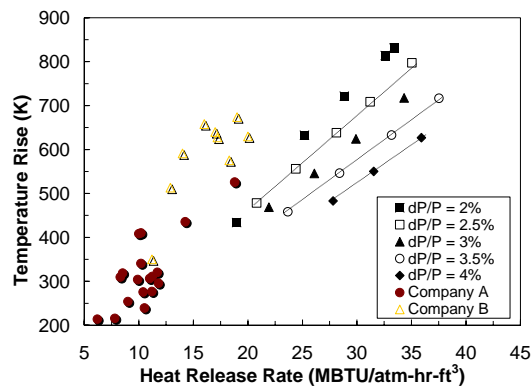


**Figure 13: Heat Release Rate for UCC Compared to Conventional Combustor Primary Zone Values.**

## Combustion Stability

Combustor lean blowout (LBO) was investigated for the different configurations. The OFAR at LBO was plotted against the cavity g-loading and cavity loading parameter (LP). To determine cavity g-loading, estimates of the tangential velocity ( $V_{tan}$ ) were estimated from previous experimental data by Quaale et al.<sup>14</sup>, and the expression;

$$g = \frac{V_{tan}^2}{g_c r_{cav}} \quad \text{Eq. (1)}$$

was used to calculate the g-loading. The cavity loading parameter (LP) is defined as;

$$LP = \frac{Wa}{\delta_{3.0}^{1.75} V_{Cav} e^{\frac{T_3}{540}}} \quad \text{Eq. (2)}$$

where,

$$\delta = \frac{P_{T3}}{14.7} \quad \text{Eq. (3)}$$

These tests were run at atmospheric pressure and 500 °F inlet air temperature.

Figure 14 and Fig. 15 show the OFAR and  $\phi_{cav}$  at blowout as a function of the cavity g-loading. In Fig. 14, the OFAR at blowout increases with cavity g-loading for all configurations from a value of OFAR ~ 0.001 at g-loads of 500 g's, to OFAR ~ 0.008 at g-loads of 4500 g's. Configuration 1 has the highest blowout values, while Configuration 3 had excellent LBO performance.

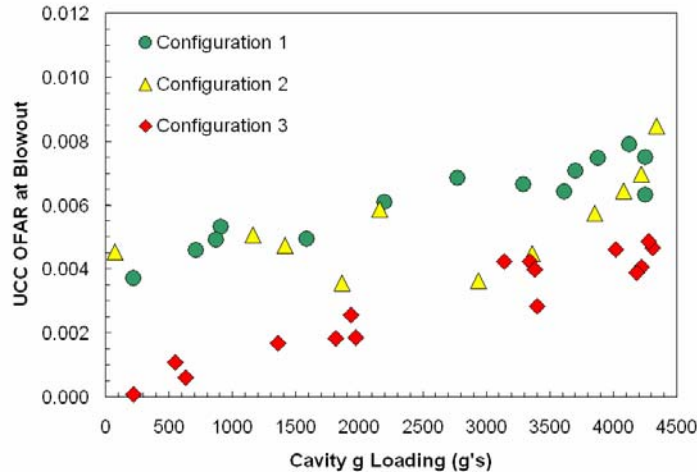


**Figure 14: Lean Blowout OFAR as a function of cavity g-loading.**

Although the combustor OFAR is a good indicator of LBO performance and can readily be compared to conventional design,  $\phi_{cav}$  is an important parameter since the flame stabilizes in the circumferential cavity and the stability is controlled by the local equivalence ratio. In Fig. 15, the range of  $\phi_{cav}$  at blowout varies from extremely low values of 0.08 for Configuration 3 to 0.65 for Configuration 1 and 2. Local geometric features in the circumferential cavity allow for the extremely low LBO values, which are below the blowout values for premixed combustors.

For completeness, the LBO data was plotted as a function of cavity loading parameter (LP). Conventional combustor designs are compared based on this parameter. Figure 16 and Fig. 17 show LBO data related to cavity LP. The cavity volume was determined from the physical dimensions of the cavity size. As expected, LBO values for both OFAR and  $\phi_{cav}$  increase with increased LP. In Fig. 15, Configuration 3 has the best LBO performance, with maximum OFAR near 0.0045 at the maximum LP. These values were two to three times lower that values seen with Configuration 1 and Configuration 2. Similarly, Fig. 16 shows values of  $\phi_{cav}$  at blowout as a function of cavity LP.

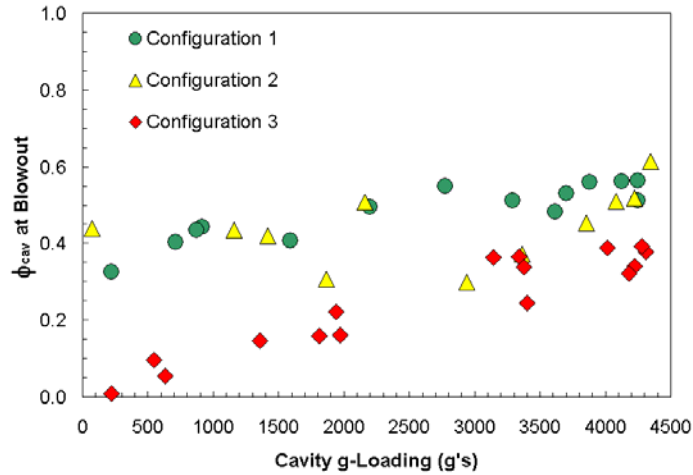


Figure 14: Lean Blowout Equivalence Ratio as a function of cavity g loading.

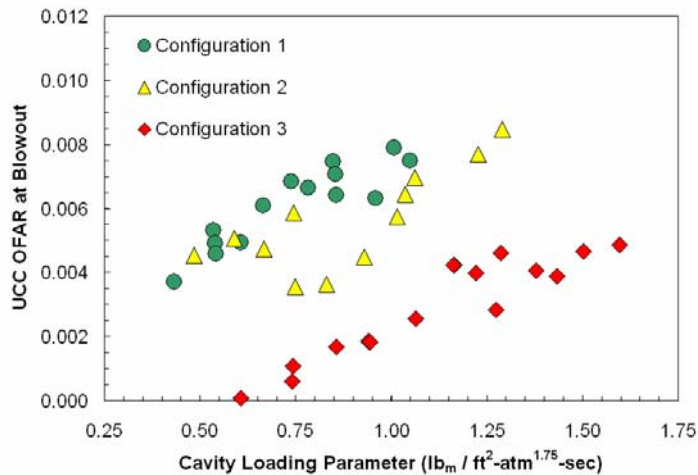
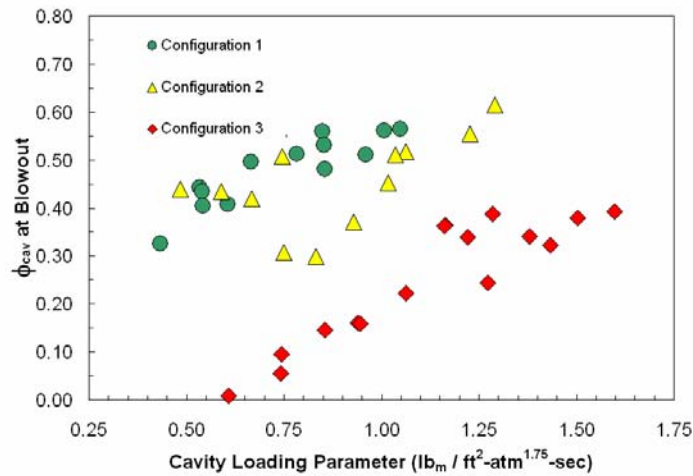


Figure 15: Lean Blowout OFAR as a function of cavity loading parameter.

**Combustion Efficiency**

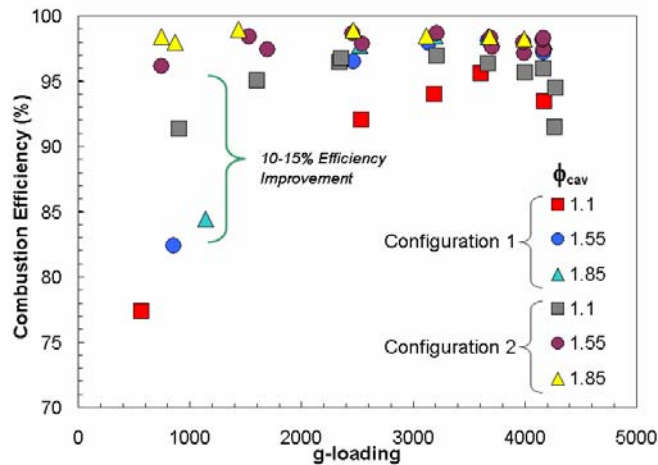
Combustion efficiency, determined by gas analysis, which is more usually plotted against LP, was here plotted as a function of the estimated g-loading in the cavity. The reason for this approach was to explore the presumption that burning rates would be enhanced by the g-loading, as will be explained below. Using Eq. 1, estimated g-loading ranged from 300 to 4500 g's depending on the operating conditions.

Figure 17 shows combustion efficiency as a function of g-loading and  $\phi_{cav}$  for Configuration 1 and Configuration 2. At  $500 < g\text{-loading} < 2500$ , Configuration 2 has superior efficiency compared to Configuration 1 at all  $\phi_{cav}$  values. The efficiency improvement is +10-15% increase in combustion efficiency. At g-loadings  $> 2500$ , the data collapses on a common curve for both configurations and all  $\phi_{cav}$ . This data suggests the improved performance of the angled RVC compared to the contoured design. The angled RVC provides additional residence time to adequately burn the fuel-air mixture and mix these products with the main airflow. This can be seen in Fig. 18b where the flame clearly is transported from the circumferential cavity to the center body of the combustion rig. The contoured RVC does not allow for efficient mixture transport to the centerline of the rig, and allows for additional spillage around the RVC and cavity exit. This is shown in Fig. 18a.



**Figure 16: Cavity Lean Blowout Equivalence Ratio as a function of cavity loading parameter.**

An interesting trend was observed when comparing results from Configurations 2 and Configuration 3 where only the amount of air flowing around the fuel injector was changed. For high airflow, the efficiency increased with  $\phi_{cav}$  to a maximum value at the highest fuel flow into the circumferential cavity. This can be seen in Fig. 19, filled data points. When injector airflow was minimized, the combustion efficiency increased to values of  $\phi_{cav} > 1.0$ , then decreased and finally increased while the circumferential cavity fueling increased to values of  $\phi_{cav} = 2.0$ . The dip in the curve was repeatable for all levels of g-loading in the cavity, however the points of inflection shifted slightly for different g-loading values. Upon further investigation of past data, visual inspection of the flame during the test runs, and preliminary CFD analysis, it was determined that the dip in the curve is due to a transition of the combustion process from the circumferential cavity, to the RVC, and finally continued reactions in the main combustion zone.



**Figure 17: Combustion efficiency as a function of g-loading and cavity equivalence ratio for the two different RVC configurations.**

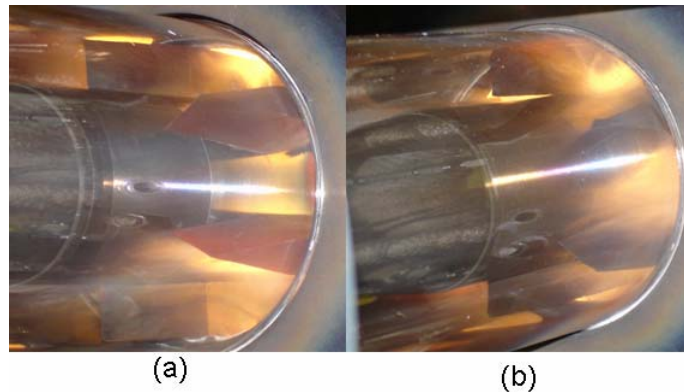


**Figure 18: Radial Vane Cavity (RVC) designs showing (a) contoured RVC and (b) angled RVC, along with the flame propagation along these RVC geometries.**

This hypothesis is illustrated more clearly in Fig. 20. The data plotted is only for the low airflow case. The red line is an estimate of all data from the high airflow case. For lean values of  $\phi_{cav}$ , the efficiency increases to a value of  $\phi_{cav} \sim 1.1$ . The flame is contained in the cavity for this fueling range. As the fuel flow is increased, combustion cannot be contained in the circumferential cavity spillage along the circumferential cavity into the main flow of unreacted fuel and air occurs, leading to quenching effects and decreased efficiency. As  $\phi_{cav}$  is increased further, the reactants begin to burn effectively in the RVC's which allow for better mixing with the main airflow and the efficiency begins to increase once again. For high injector airflow, the fuel is immediately transported to the RVC and the main flow, via momentum of this airstream, and is not completely contained in the circumferential cavity. This transport and ultimately quenching of reactants in the RVC and main airflow lead to poor efficiency at fuel-lean conditions.

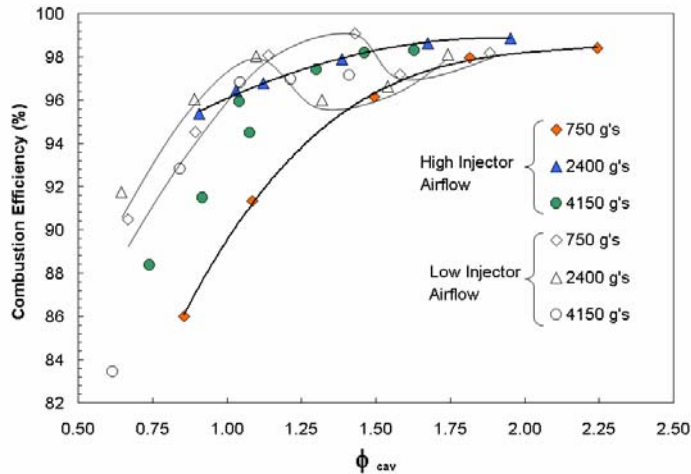


**Figure 19: Combustion efficiency as a function of circumferential cavity g-loading and amount of airflow around fuel injection locations.**

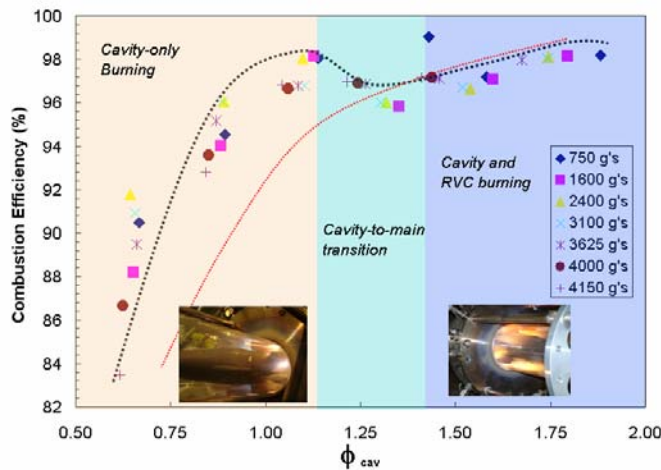
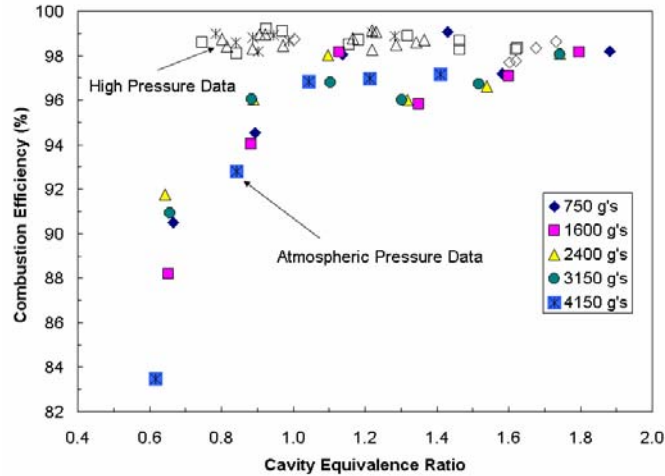


**Figure 20: Combustion efficiency as a function of g-loading and cavity equivalence ratio for the two different injector airflow configurations.**

### **Pressure Effects**

Initial performance of the combustor configurations were conducted in the APCRC, however, the UCC will operate at elevated pressure. Therefore, the UCC was operated at elevated pressures, in the range of 40 to 60 psia, for the Configuration 3 design<sup>15</sup>. Inlet temperature remained the same as the APCRC tests, at 500° F. A comparison of both the combustion efficiency and the lean blowout values were made for atmospheric and elevated pressure conditions. It is expected that the combustion efficiency would improve at high pressure due to the increased reaction rates as expressed by the Arrhenius equation<sup>13</sup>.

In Fig. 21, the combustion efficiency as a function of g-loading and  $\phi_{cav}$  is shown. At  $\phi_{cav} > 1.2$ , the combustion efficiency for the atmospheric pressure case is considerably lower than the elevated pressure condition. As  $\phi_{cav}$  increases, the two curves converge to a similar combustion efficiency level. These results are encouraging, since it shows that the combustor performance at pressure will provide an efficient system.



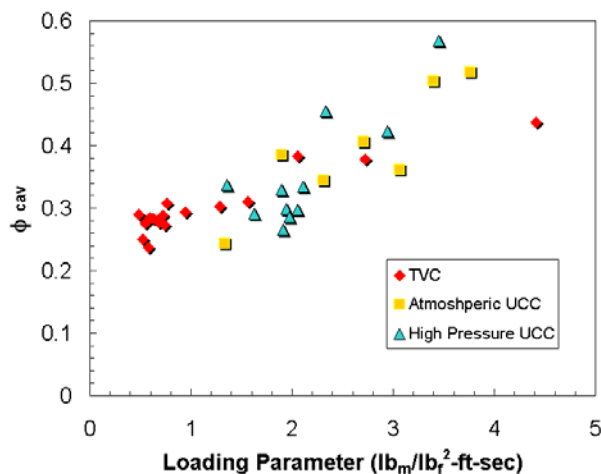
**Figure 21: Pressure effects on combustion efficiency as a function of cavity equivalence ratio and g-loading.**

Figure 22 shows a comparison of the  $\phi_{cav}$  value at blowout for the high pressure and atmospheric pressure data, along with data from the TVC<sup>1</sup>. Of interest is the fact that the UCC and TVC have very similar LBO performance. It is also observed that the pressure has little effect on the combustor LBO limits. As with pressure, this is expected since the pressure dependence as expressed in the Arrhenius equation decreases as  $\phi_{cav}$  approaches the LBO limit<sup>16</sup>.

### **Pollutant Emissions**

Another indicator of combustion system performance is the amount of pollutants emitted. A typical NO<sub>x</sub> – CO emissions trade is shown for the three test configurations in Fig. 23. Plotting emissions in this fashion allow for investigation of true emissions technology improvements versus NO<sub>x</sub>-CO trades.

Configuration 2 and Configuration 3 showed very similar NO<sub>x</sub>-CO trade curves, with maximum CO occurring at minimum NO<sub>x</sub> values. Configuration 3 had slightly lower NO<sub>x</sub> and CO values compared to the Configuration 2 data. Configuration 1 however, showed similar values of maximum NO<sub>x</sub> values while exhibiting much lower CO levels. In fact, CO values were about half of those seen in Configuration 2 and Configuration 3. From a first look, it would seem that Configuration 1 had the best emission performance, but investigation of other emissions values showed that this was not the case.



**Figure 22: Pressure effects on cavity equivalence ratio lean blowout limits as a function of cavity g-loading.**

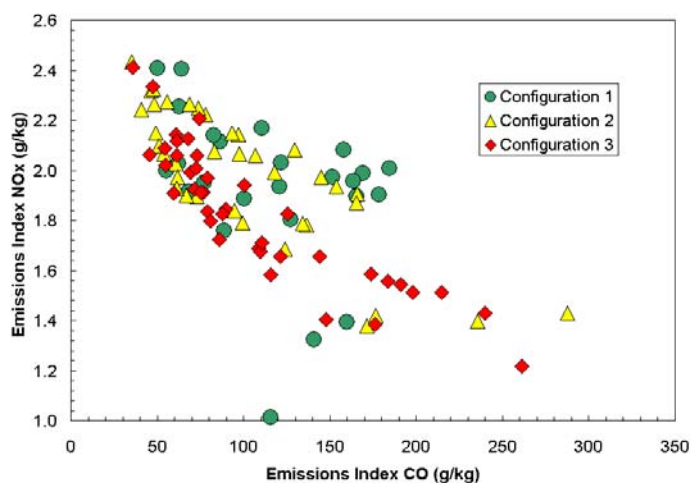


**Figure 23: NO<sub>x</sub>-CO emissions trades for the three test configurations.**

Plotting the unburned hydrocarbon (UHC) emissions along with the CO data, as seen in Fig. 24, shows that Configuration 1 had much higher UHC levels. The reactions from hydrocarbons to CO were quenched in this configuration, leading to low CO levels but very high UHC levels. The combination of the contoured RVC, which did not promote mixing in the main flow, along with the high airflow admitted around the fuel injector, forced the unreacted fuel into the relatively cool main airstream where the reactions were quenched. Figure 24 also shows that Configuration 3 lower CO emissions while maintaining about the same UHC levels compared to Configuration 2. Although the CO and UHC levels are quite high for some of the operating conditions tested, it must be kept in mind that the maximum CO and UHC emissions occurred at OFAR  $\sim 0.0075$ , near the LBO limit of most conventional combustion systems.

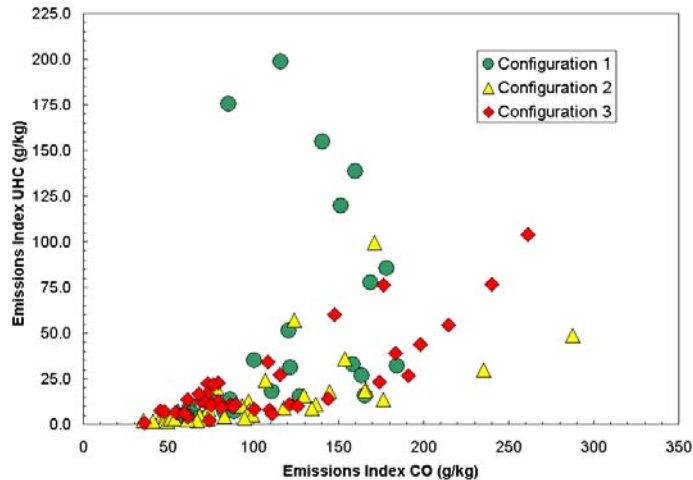


**Figure 24: UHC-CO emissions trades for the three test configurations.**

## CONCLUSIONS

An experimental investigation of a high g-loaded combustion system has been successfully conducted in an atmospheric pressure rig. Parameters investigated included amount of fuel injector air and the use of a radial vane cavity along the turbine vanes. The results indicate that this type of combustion system has the potential to be used as an ultra-compact combustor (UCC) for a main burner, or an inter-turbine burner (ITB) for use as a reheat cycle engine. Key features of the combustion system include:

1. Short combustion lengths estimated at 50% of conventional combustion systems operating at similar conditions.
2. Excellent LBO performance that, for some configurations, is independent of combustor loading parameter. In fact, the UCC LP is two to four times that of conventional systems while still maintaining the same or lower LBO levels.
3. A trade exists between the cavity extraction via radial vane cavities which impact combustion efficiency, temperature distribution, and LBO. Optimization of the radial vane cavity, the circumferential cavity, and the fuel injection scheme is needed to balance this trade between combustion performance parameters.
4. Physical processes occurring in the cavity indicate that the un-reacted mixture transport into the main airflow is a strong function of injector air and cavity g-loading. Increased g-loads create a centrifuge effect in the cavity, keeping un-reacted mixture toward the cavity OD. However, a limit is reached where flame extinction occurs in the cavity due to high velocities which are unable to sustain the flame. Therefore, a window of optimal g-loading appears to be 500-3500 g's. Higher g-loads result in an efficiency degradation.
5. Pressure effects improve the combustion efficiency for a given configuration, but have little impact on the lean blowout performance.

Additional tests are planned at high-pressure conditions to understand the impact of pressure on the combustion system performance. Investigation of the UCC for use as a main combustor, or as an ITB for a reheat cycle is underway.

## REFERENCES

1. Roquemore, W.M., Shouse, D., Burrus, D., Johnson, A., Cooper, C., Duncan, B, Hsu, K-Y, Katta, V.R., Sturgess, G.J. & Vihinen, I., "Trapped Vortex Combustor Concept for Gas Turbine Engines," AIAA-2001-0483.
2. Hsu, K-Y, Goss, L.P. & Roquemore, W.M., "Characteristics of a Trapped-Vortex Combustor," *Journal of Propulsion and Power*, Vol. 14, No. 1, 1998, p. 57.
3. Roquemore, W.M., Vihinen, I., Hartrauft, J. & Mantis, P.M., "Trapped Vortex Combustor for Gas Turbine Engines," Annual Report to SERDP, 1998.
4. Anthenien, R. A., Mantz, R. A., Roquemore, W. M., and Sturgess, G. J., "Experimental Results for a Novel, High Swirl, Ultra Compact Combustor for Gas Turbine Engines," 2nd Joint Meeting of the U.S. Sections of the Combustion Institute, Oakland, CA March 2001.
5. Zelina, J., Ehret, J., Hancock, R. D., Shouse, D. T., Sturgess, G. J., and Roquemore, W. M., "Ultra-Compact Combustion Technology Using High Swirl to Enhance Burning Rate," AIAA 2002-3725.
6. Zelina, J., Sturgess, G. J., Mansour, A., and Hancock, R. D., "Fuel Injection Design for Ultra-Compact Combustor," ISABE 2003-1089.
7. Zelina, J., Shouse, D. T., and Hancock, R. D., "Ultra-Compact Combustors for Advanced Gas Turbine Engines," ASME IGTI 2004-GT-53155.
8. Zelina, J., Sturgess, G. J and Shouse, D. T., "The Behavior of an Ultra-Compact Combustor (UCC) Based on Centrifugally-Enhanced Turbulent Burning Rates," AIAA 2004-3541.
9. Lewis, G.D., "Centrifugal-Force Effects on Combustion," proc. 14<sup>th</sup>. *Symposium (International) on Combustion*, The Combustion Institute, 1973, pp. 413-419.
10. Katta, V. R., model results and private communications.
11. Yonezawa, Y., Toh, H., Goto, S., and Obata, M., "Development of the Jet-Swirl High Loading Combustor," 26<sup>th</sup> *AIAA/SAE/ASME/ASEE Joint Propulsion Conference*, Orlando, FL, AIAA-90-2451, 1990.
12. Chomiak, J., "Dissipation Fluctuations and the Structure and Propagation of Turbulent Flames in Premixed Gases at High Reynolds Numbers," Sixteenth Symposium (International) on Combustion, The Combustion Institute, 1977, pp. 1665-1673.
13. Sturgess, G.J., Lecture notes on *Advanced Aircraft Engine Design, Vol. II*, Pratt & Whitney, presented at Institute and Department of Aeronautics and Astronautics, National Cheng Kung University, Tainan, Taiwan, R.O.C., May 24-26, 1994.
14. Quaale, R. J., Anthenien, R. A., Zelina, J., Ehret, J., "Flow Measurements Within a High Swirl Ultra Compact Combustor for Gas Turbine Engines," ISABE 2003-1141.
15. Zelina, J., Shouse, D. T., and Neuroth C., "High Pressure Tests of a High-g Ultra-Compact Combustor," AIAA 2005-3779.
16. Lefebvre, A. H., "Gas Turbine Combustor Short Course" Lecture Notes, Irvine, CA, March 1997.

## NOMENCLATURE

EI = Emissions Index (g-pollutant/kg-fuel)  
g = g loading  
g<sub>c</sub> = Newton's constant (lbf ft)/(lbf s<sup>2</sup>)  
ITB = Inter-Turbine Burner  
LP = loading parameter (lbf/ft<sup>3</sup>-atm<sup>1.75</sup>-s)  
OFAR = overall fuel-air ratio  
P<sub>T</sub> = total pressure (psia)  
T = temperature (°R)  
TVC = Trapped Vortex Combustor  
r = radius  
UCC = Ultra-Compact Combustor  
V = velocity (ft/sec)  
V<sub>c</sub> = reaction volume (ft<sup>3</sup>)  
W<sub>a</sub> = mass flowrate (lbf/sec)  
φ = metered equivalence ratio

## Subscripts

cav = cavity  
tan = tangential component  
3 = Station 3, Combustor Inlet